IOPscience iopscience.iop.org

Home Search Collections Journals About Contact us My IOPscience

Structure of glassy GeO_2

This article has been downloaded from IOPscience. Please scroll down to see the full text article.

2007 J. Phys.: Condens. Matter 19 415110

(http://iopscience.iop.org/0953-8984/19/41/415110)

View the table of contents for this issue, or go to the journal homepage for more

Download details:
IP Address: 129.252.86.83
The article was downloaded on 29/05/2010 at 06:12

Please note that terms and conditions apply.

IOP PUBLISHING JOURNAL OF PHYSICS: CONDENSED MATTER

J. Phys.: Condens. Matter **19** (2007) 415110 (22pp) doi:10.1088/0953-8984/19/41/415110

Structure of glassy GeO_2

Philip S Salmon[1], Adrian C Barnes[2], Richard A Martin[1] and Gabriel J Cuello[3]

[1] Department of Physics, University of Bath, Bath BA2 7AY, UK
[2] H H Wills Physics Laboratory, Royal Fort, Tyndall Avenue, University of Bristol, BS8 1TL, UK
[3] Institut Laue-Langevin, BP 156, F-38042, Grenoble Cédex 9, France

Received 5 May 2007, in final form 7 May 2007
Published 27 September 2007
Online at stacks.iop.org/JPhysCM/19/415110

Abstract

The full set of partial structure factors for glassy germania, or GeO_2, were accurately measured by using the method of isotopic substitution in neutron diffraction in order to elucidate the nature of the pair correlations for this archetypal strong glass former. The results show that the basic tetrahedral $Ge(O_{1/2})_4$ building blocks share corners with a mean inter-tetrahedral Ge–$\hat{O}$–Ge bond angle of 132(2)°. The topological and chemical ordering in the resultant network displays *two* characteristic length scales at distances greater than the nearest neighbour. One of these describes the intermediate range order, and manifests itself by the appearance of a first sharp diffraction peak in the measured diffraction patterns at a scattering vector $k_{\mathrm{FSDP}} \approx 1.53$ Å^{-1}, while the other describes so-called extended range order, and is associated with the principal peak at $k_{\mathrm{PP}} = 2.66(1)$ Å^{-1}. We find that there is an interplay between the relative importance of the ordering on these length scales for tetrahedral network forming glasses that is dominated by the extended range ordering with increasing glass fragility. The measured partial structure factors for glassy GeO_2 are used to reproduce the total structure factor measured by using high energy x-ray diffraction and the experimental results are also compared to those obtained by using classical and first principles molecular dynamics simulations.

(Some figures in this article are in colour only in the electronic version)

1. Introduction

Germania (GeO_2) is, like silica (SiO_2), an archetypal 'strong' glass forming material, a taxonomy which stems originally from the Arrhenius temperature dependence observed for the liquid viscosity η and which can be usefully used to describe many of the generic properties of glass forming systems [1]. For strong liquids, a plot of $\ln \eta$ versus T_g/T gives a straight line, where T is the absolute temperature and T_g is the glass transition temperature, whereas large deviations from linearity are found for fragile liquids. Strong liquids, by contrast to their fragile counterparts, commonly show a small change of heat capacity at T_g corresponding to

a small change in the configurational entropy with temperature as the liquid solidifies into the glassy phase [2]. Computer simulation studies show quantitative differences between the potential energy landscapes of strong and fragile liquids that help to rationalize the experimental observations [3–6].

There is evidence to suggest that the concept of fragility can be related to the microscopic properties of a glass [7]. A correlation between the fragility of a glass forming liquid and the Poisson ratio of the corresponding glass has also been reported [8], although later work casts doubt on the reliability of this finding [9]. Strong liquids and glasses like GeO_2 and SiO_2 form network structures which eventually collapse with increasing density and there is often an accompanying increase in the number of structural configurations that can be adopted. For example, whereas the network of glassy GeO_2 at ambient conditions is built predominantly from Ge-centred tetrahedral units, the Ge coordination number increases to six at higher pressures [10–13]. Strong systems tend to become more fragile with increase of density [4, 14, 15].

It is therefore important to understand the relation between the structure and relative fragility of glass forming systems. Detailed information on the former is, however, notable by its paucity, especially at length scales greater than the nearest neighbour which determine many important aspects of liquid and glass phenomenology [16]. Recently, progress has been made by employing the method of isotopic substitution in neutron diffraction to measure the full set of partial structure factors for two network forming AX_2 glasses, namely $GeSe_2$ [17, 18] and $ZnCl_2$ [19]. By constructing the Bhatia–Thornton partial structure factors [20], the topological and chemical ordering was examined and at distances greater than the nearest neighbour, *two* length scales associated with the atomic ordering were identified [19]. One of these is associated with an *intermediate* range and manifests itself by the appearance in the measured diffraction patterns of a first sharp diffraction peak (FSDP) at a scattering vector $k_{\rm FSDP} \approx 1$ Å^{-1}. The other is associated with an *extended* range which has a periodicity given by $\approx 2\pi/k_{\rm PP}$ where $k_{\rm PP}$ is the position of the principal peak at $\approx$2.1 Å^{-1}. It is therefore crucial to understand how this ordering affects the system properties e.g. in the case of network forming ionic melts the density fluctuations relax much more slowly on length scales associated with the FSDP compared with the principal peak [21]. In particular, what distinguishes the structure of a strong glass such as GeO_2 or SiO_2 from that of $ZnCl_2$ and $GeSe_2$ which are much more 'intermediate' in character given that the dominant structural motif in all these systems is the $A(X_{1/2})_4$ tetrahedron?

We have therefore taken advantage of advances in neutron diffraction instrumentation [22] to apply the method of isotopic substitution [23] to make the first accurate measurement of the full set of partial structure factors for GeO_2. Although these functions have previously been estimated for GeO_2, by combining one neutron diffraction pattern with two x-ray diffraction patterns measured using anomalous scattering, the results are prone to systematic error and, even in the most recent work, significant unphysical features can be identified [24–26]. For example, the published partial structure factors correspond to a negative measured intensity in the region of the FSDP [26] and the results have not allowed for a detailed investigation of the glass structure at distances beyond the nearest neighbour. The partial structure factors for glassy GeO_2 have also been calculated from neutron and x-ray diffraction data by using reverse Monte Carlo modelling [27–29]. This modelling procedure tends, however, to produce the most disordered structure that is consistent with the data and imposed constraints [30] and, in the most recent work, only two diffraction patterns were used in the refinement procedure. The structure of amorphous, crystalline and liquid GeO_2 has recently been reviewed by Micoulaut *et al* [31] and the use of germania glass for fibre optics is described by Dianov

and Mashinsky [32]. A preliminary account of the present work on glassy GeO_2 is given elsewhere [33].

The manuscript is organized as follows. Firstly, the theory that is required to understand the experimental results is given, followed by the method of sample preparation and the neutron diffraction experimental procedure. Next, the neutron diffraction results, at both the first order difference function and partial structure factor levels, are presented. The structure of glassy GeO_2 on different length scales is then discussed and, to help elucidate the interpretation of x-ray and neutron diffraction patterns taken under extreme conditions, the x-ray and neutron total structure factors are reconstructed by using the measured partial structure factors. The results for GeO_2 are compared with those recently obtained by using classical [34–37] and first principles molecular dynamics simulations [38, 39]. Finally, the results are also compared with the structure of SiO_2, with the structure of glassy GeO_2 under pressure, and with the structure of other tetrahedral network forming glasses such as $ZnCl_2$ and $GeSe_2$. The comparison suggests that there is a competition between the ordering on the intermediate and extended length scales which is won by the extended range order with increasing glass fragility.

2. Theory

In a neutron diffraction experiment on glassy GeO_2 the coherent scattered intensity can be represented by the total structure factor [40]

$$F(k) = c_{\mathrm{Ge}}^2 b_{\mathrm{Ge}}^2 [S_{\mathrm{GeGe}}(k) - 1] + 2c_{\mathrm{Ge}}c_{\mathrm{O}}b_{\mathrm{Ge}}b_{\mathrm{O}}[S_{\mathrm{GeO}}(k) - 1] + c_{\mathrm{O}}^2 b_{\mathrm{O}}^2 [S_{\mathrm{OO}}(k) - 1] \quad (1)$$

where $S_{\alpha\beta}(k)$ represents a Faber–Ziman [41] partial structure factor and c_α, b_α denote the atomic fraction and bound coherent scattering length of chemical species α, respectively. Let the diffraction patterns be measured for three samples denoted by $^{\mathrm{nat}}GeO_2$, $^{70}GeO_2$ and $^{73}GeO_2$ that are identical in every respect except for their Ge isotope composition, where nat denotes the natural isotopic abundance of germanium. The corresponding total structure factors, denoted by $^{\mathrm{nat}}F(k)$, $^{70}F(k)$ and $^{73}F(k)$ respectively, can then be represented in matrix notation by

$$\begin{bmatrix} {}^{\mathrm{nat}}F(k) \\ {}^{70}F(k) \\ {}^{73}F(k) \end{bmatrix} = \begin{bmatrix} 0.0744(4) & 0.2111(5) & 0.1497(2) \\ 0.1097(21) & 0.2563(25) & 0.1497(2) \\ 0.0297(4) & 0.1334(10) & 0.1497(2) \end{bmatrix} \begin{bmatrix} S_{\mathrm{GeGe}}(k) - 1 \\ S_{\mathrm{GeO}}(k) - 1 \\ S_{\mathrm{OO}}(k) - 1 \end{bmatrix} \quad (2)$$

where the weighting coefficients of the $S_{\alpha\beta}(k)$ are quoted in units of barns (1 barn $= 10^{-28}$ m^2) and were calculated by using $b(^{70}\mathrm{Ge}) \equiv {}'b_{\mathrm{Ge}} = 9.94(10)$, $b(^{\mathrm{nat}}\mathrm{Ge}) \equiv {}''b_{\mathrm{Ge}} = 8.185(20)$ and $b(^{73}\mathrm{Ge}) \equiv {}'''b_{\mathrm{Ge}} = 5.17(4)$ fm, which correspond to the isotopic enrichments used in the neutron diffraction experiment (see section 3), and $b_{\mathrm{O}} = 5.803(4)$ fm [42].

By using two total structure factors it is possible to eliminate, for instance, the O–O correlations by forming a first order difference function such as

$$\begin{aligned} \Delta F_{\mathrm{Ge}}^{(1)}(k) &= {}^{70}F(k) - {}^{73}F(k) \\ &= c_{\mathrm{Ge}}^2({}'b_{\mathrm{Ge}}^2 - {}'''b_{\mathrm{Ge}}^2)[S_{\mathrm{GeGe}}(k) - 1] + 2c_{\mathrm{Ge}}c_{\mathrm{O}}b_{\mathrm{O}}({}'b_{\mathrm{Ge}} - {}'''b_{\mathrm{Ge}})[S_{\mathrm{GeO}}(k) - 1] \end{aligned} \quad (3)$$

where the Ge–Ge and Ge–O weighting factors take values of 0.080(2) and 0.123(3) barns, respectively. Equivalent expressions hold for $\Delta F_{\mathrm{Ge}}^{(2)}(k) = {}^{70}F(k) - {}^{\mathrm{nat}}F(k)$ and $\Delta F_{\mathrm{Ge}}^{(3)}(k) = {}^{\mathrm{nat}}F(k) - {}^{73}F(k)$. The full set of partial structure factors is obtained by inverting the scattering matrix given by equation (2) to give

$$\begin{bmatrix} S_{\mathrm{GeGe}}(k) - 1 \\ S_{\mathrm{GeO}}(k) - 1 \\ S_{\mathrm{OO}}(k) - 1 \end{bmatrix} = \begin{bmatrix} -170.7 & 107.9 & 62.8 \\ 111.1 & -62.1 & -49.0 \\ -65.2 & 33.9 & 37.9 \end{bmatrix} \begin{bmatrix} {}^{\mathrm{nat}}F(k) \\ {}^{70}F(k) \\ {}^{73}F(k) \end{bmatrix}. \quad (4)$$

A measure of the conditioning of this matrix is provided by its normalized determinant $|A_n| = -0.006$ [43]. This value compares, for example, with $|A_n| = 0.011$ for the experiment

of Petri *et al* [17, 18] on glassy $GeSe_2$ in which the full set of $S_{\alpha\beta}(k)$ were successfully measured by using the method of isotopic substitution in neutron diffraction. Extraction of the full set of partial structure factors for GeO_2 is therefore more challenging than for $GeSe_2$.

The partial structure factors are related to the partial pair distribution functions, $g_{\alpha\beta}(r)$, through

$$g_{\alpha\beta}(r) = 1 + \frac{1}{2\pi^2 n_0 r}\int_0^\infty \mathrm{d}k\, k[S_{\alpha\beta}(k) - 1]\sin(kr) \tag{5}$$

where $n_0 (= 0.0629(3)\ \text{Å}^{-3}$ [44]) is the atomic number density of the glass. The total pair distribution function corresponding to equation (1) is therefore given by

$$G(r) = c_{\mathrm{Ge}}^2 b_{\mathrm{Ge}}^2[g_{\mathrm{GeGe}}(r) - 1] + 2c_{\mathrm{Ge}}c_{\mathrm{O}}b_{\mathrm{Ge}}b_{\mathrm{O}}[g_{\mathrm{GeO}}(r) - 1] + c_{\mathrm{O}}^2 b_{\mathrm{O}}^2[g_{\mathrm{OO}}(r) - 1] \tag{6}$$

and the real space difference function corresponding to equation (3) is given by

$$\Delta G_{\mathrm{Ge}}^{(1)}(r) = c_{\mathrm{Ge}}^2({}'b_{\mathrm{Ge}}^2 - {}'''b_{\mathrm{Ge}}^2)[g_{\mathrm{GeGe}}(r) - 1] + 2c_{\mathrm{Ge}}c_{\mathrm{O}}b_{\mathrm{O}}({}'b_{\mathrm{Ge}} - {}'''b_{\mathrm{Ge}})[g_{\mathrm{GeO}}(r) - 1]. \tag{7}$$

The mean number of particles of type β contained in a volume defined by two concentric spheres of radii r_i and r_j, centred on a particle of type α, is given by

$$\bar{n}_\alpha^\beta = 4\pi n_0 c_\beta \int_{r_i}^{r_j} \mathrm{d}r\, r^2 g_{\alpha\beta}(r). \tag{8}$$

In practice, the measured reciprocal space data sets will be truncated at some finite maximum value $k_{\max}$ owing to the finite measurement window function $M(k)$ of the diffractometer. In consequence, equation (5) needs to be modified and it is convenient to rewrite it as

$$d'_{\alpha\beta}(r) = \frac{2}{\pi}\int_0^\infty \mathrm{d}k\, k[S_{\alpha\beta}(k) - 1]M(k)\sin(kr) = d_{\alpha\beta}(r) \otimes M(r) \tag{9}$$

where $d_{\alpha\beta}(r) = 4\pi n_0 r[g_{\alpha\beta}(r) - 1]$ and $\otimes$ denotes the one-dimensional convolution operator. The $d_{\alpha\beta}(r)$ functions are then convoluted with a symmetrical $M(r)$ function. For example, the measurement window is usually represented by the step function $M(k \leqslant k_{\max}) = 1, M(k > k_{\max}) = 0$ whence $M(r) = k_{\max}\,\mathrm{sinc}(k_{\max}r)/\pi$ with $\mathrm{sinc}(x) \equiv \sin(x)/x$. Alternatively, the adoption of a Lorch [45] modification function $M(k) = \sin(ak)/(ak)$ where $a = \pi/k_{\max}$ gives $M(r) = [\mathrm{Si}(\pi(r + a)/a) - \mathrm{Si}(\pi(r - a)/a)]/2\pi a$ where the sine integral $\mathrm{Si}(x) \equiv \int_0^x \sin(t)/t\ \mathrm{d}t$ [46]. Application of this modification function gives smoother pair correlation functions at all r values by comparison with the use of a step modification function but leads to a loss in resolution of the first peaks in r-space.

A total structure factor can also be written in terms of the Bhatia–Thornton [20] number–number, concentration–concentration and number–concentration partial structure factors, denoted by $S_{\mathrm{NN}}(k)$, $S_{\mathrm{CC}}(k)$ and $S_{\mathrm{NC}}(k)$ respectively, where

$$\begin{aligned} F(k) = {} & \langle b\rangle^2[S_{\mathrm{NN}}(k) - 1] + c_{\mathrm{Ge}}c_{\mathrm{O}}(b_{\mathrm{Ge}} - b_{\mathrm{O}})^2[\{S_{\mathrm{CC}}(k)/c_{\mathrm{Ge}}c_{\mathrm{O}}\} - 1] \\ & + 2\langle b\rangle(b_{\mathrm{Ge}} - b_{\mathrm{O}})S_{\mathrm{NC}}(k) \end{aligned} \tag{10}$$

and $\langle b\rangle = c_{\mathrm{Ge}}b_{\mathrm{Ge}} + c_{\mathrm{O}}b_{\mathrm{O}}$ is the average scattering length. If the scattering matrix of equation (2) is rewritten in terms of the Bhatia–Thornton $S_{IJ}(k)$ (where $I, J = \mathrm{N}, \mathrm{C}$) then the corresponding normalized determinant $|A_n| = 0.016$ i.e. the conditioning of the Bhatia–Thornton partial structure factors is better than for the corresponding Faber–Ziman partial structure factors. The relationship between these two sets of partial structure factors is given by

$$\begin{aligned} S_{\mathrm{NN}}(k) &= c_{\mathrm{Ge}}^2 S_{\mathrm{GeGe}}(k) + c_{\mathrm{O}}^2 S_{\mathrm{OO}}(k) + 2c_{\mathrm{Ge}}c_{\mathrm{O}}S_{\mathrm{GeO}}(k) \\ S_{\mathrm{CC}}(k) &= c_{\mathrm{Ge}}c_{\mathrm{O}}[1 + c_{\mathrm{Ge}}c_{\mathrm{O}}(S_{\mathrm{GeGe}}(k) + S_{\mathrm{OO}}(k) - 2S_{\mathrm{GeO}}(k))] \\ S_{\mathrm{NC}}(k) &= c_{\mathrm{Ge}}c_{\mathrm{O}}[c_{\mathrm{Ge}}(S_{\mathrm{GeGe}}(k) - S_{\mathrm{GeO}}(k)) - c_{\mathrm{O}}(S_{\mathrm{OO}}(k) - S_{\mathrm{GeO}}(k))]. \end{aligned} \tag{11}$$

If $b_{Ge} = b_O$ then the incident neutrons in a diffraction experiment cannot distinguish between the different scattering nuclei and inspection of equation (10) shows that the measured total structure factor gives $S_{NN}(k)$ directly. The Fourier transform of $S_{NN}(k)$, the partial pair distribution function $g_{NN}(r)$, describes the sites of the scattering nuclei, but does not distinguish between the chemical species that decorate those sites, and therefore gives information on the topological ordering in the glass. If $\langle b \rangle = 0$, however, the measured total structure factor will give $S_{CC}(k)$ directly. The Fourier transform of $S_{CC}(k)$, namely $g_{CC}(r)$, describes the chemical ordering of the Ge and O atomic species. When there is a preference for like or unlike neighbours at a given distance, corresponding positive or negative peaks will appear in $g_{CC}(r)$ respectively. The Fourier transform of $S_{NC}(k)$, namely $g_{NC}(r)$, describes the correlation between the sites described by $g_{NN}(r)$ and their occupancy by a given chemical species. A more complete description of 2:1 binary systems using the Bhatia–Thornton formalism is given elsewhere [47].

3. Experimental procedure

Germania glasses were made by heating ≈1.35 g of powdered $^{nat}GeO_2$ (99.9999%, Alfa Aesar), $^{70}GeO_2$ (97.22% enrichment) or $^{73}GeO_2$ (95.51% enrichment) contained in platinum crucibles (supported by an alumina crucible) at 1400 °C. The crucibles were heated in air in order to minimize any change of sample stoichiometry which is increased if inert gas conditions are used [48]. After ≈2 h, the crucibles were removed from the furnace and placed on a copper block to cool to room temperature. The transparent, colourless samples are hygroscopic and were therefore stored under dry conditions. A sample of commercial silica of natural isotopic abundance was also chosen for investigation and the number density of this glass $n_0 = 0.0665(2)$ Å^{-3}.

The diffraction experiments were made using the D4C instrument [22] at the Institut Laue-Langevin (ILL), Grenoble, operating with an incident wavelength of 0.49991(2) Å. The samples were coarsely powdered and were held in a cylindrical vanadium container of 4.8 mm internal diameter and 0.1 mm wall thickness. Diffraction patterns were taken for the samples at 25(1) °C in their container, the empty container, the empty instrument, and a cylindrical vanadium rod of diameter 6.35 mm for normalization purposes. Each diffraction pattern was built up by making repeated scans of the detectors over the available range of scattering angles. No deviations were observed between scans, apart from the expected statistical variations [49]. The intensity for a bar of neutron absorbing $^{10}B_4C$ with dimensions comparable to the sample was also measured to account for the effect of sample self-shielding on the background count rate at small scattering angles [50]. The data were carefully corrected to yield the total structure factor for each sample and the usual self-consistency checks were performed [18, 51].

4. Results

The measured total structure factors are illustrated in figure 1 and the corresponding total pair distribution functions are given in figure 2. As shown in these figures, good agreement is found with the previous measurements of Desa *et al* [52] who studied the total structure factor of $^{nat}GeO_2$ by using an earlier version of the diffractometer D4 at the ILL with an incident wavelength of 0.5 Å. The results for the $F(k)$ functions given in figure 1 show that as the scattering length of Ge decreases, the intensity of the first sharp diffraction peak at $k_{FSDP} = 1.53(2)$ Å^{-1} decreases whereas the intensity of the principal peak at $k_{PP} \approx 2.67$ Å^{-1} increases. The results for the corresponding $G(r)$ functions given in figure 2 show the extent to which the smoothing achieved by use of a Lorch modification function, relative to a step

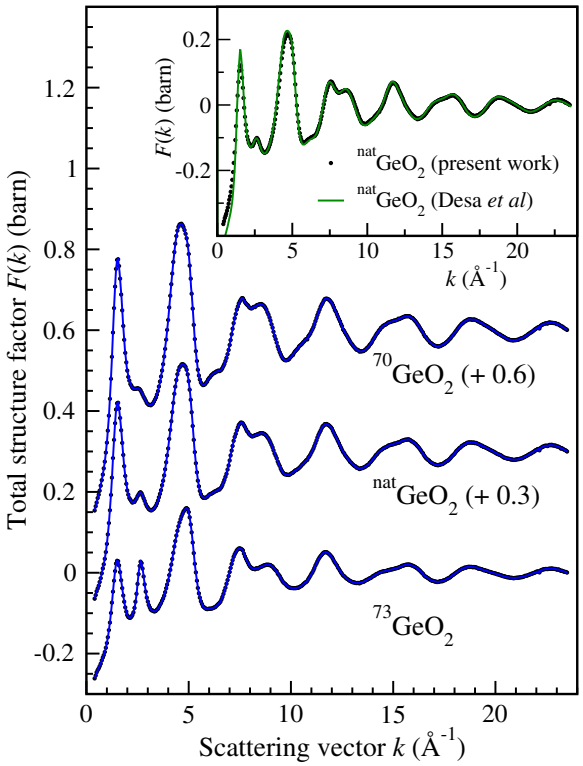

Figure 1. The measured total structure factors, $F(k)$, for glassy GeO_2 at 25(1) °C. The solid circles give the data points and are larger than the statistical errors. The solid curves give the result of recombining the $S_{\alpha\beta}(k)$ given by the solid (blue) curves in figure 5. The inset compares $^{\rm nat}F(k)$ as measured in the present work (solid circles) with the results of Desa *et al* [52] (solid curve).

modification function, comes at the expense of a loss in resolution which can be readily discerned up to ≈5 Å.

The FSDP remains as a prominent feature at ≈1.54 $Å^{-1}$ in the first order difference functions $\Delta F^{(i)}_{\rm Ge}$ (see figure 3). This demonstrates that the intermediate ranged atomic ordering in GeO_2 has a strong contribution from the correlations involving Ge atoms. The real space difference function $\Delta G^{(1)}_{\rm Ge}$ is shown in figure 4. By comparison with the structure of crystalline GeO_2 [31] the first peak at 1.73(1) Å will arise from Ge–O correlations and a fit to this peak, taking the window function $M(k)$ into account (see equation (9)), gives $\bar{n}^{\rm O}_{\rm Ge} = 3.8(1)$. As will be shown by the full partial pair distribution function analysis of the data, the second and third peaks in $\Delta G^{(1)}_{\rm Ge}$ at 3.16(2) and 4.43(2) Å have a strong contribution from $g_{\rm GeGe}(r)$ and $g_{\rm GeO}(r)$ respectively.

The partial structure factors $S_{\alpha\beta}(k)$ of figure 5 were obtained from the total structure factors $F(k)$ of figure 1 by direct inversion of the scattering matrix (see equation (4)) which means that the total structure factors can be accurately reconstructed from the $S_{\alpha\beta}(k)$ by using equation (2). The $S_{\alpha\beta}(k)$ are of high statistical quality, fully satisfy the sum rule and inequality relations given by Edwards *et al* [43], and give rise to $g_{\alpha\beta}(r)$ functions that oscillate about the correct low r limit of $g_{\alpha\beta}(r) = 0$. The $S_{\alpha\beta}(k)$ are also in good agreement at all k values with the Fourier back-transforms of the corresponding $g_{\alpha\beta}(r)$ after the low r oscillations are set to this limit, which indicates correct normalization of the data sets [53]. Furthermore, although the $S_{{\rm Ge}\beta}(k)$ functions are the least well conditioned of the set of three, they can be used to accurately

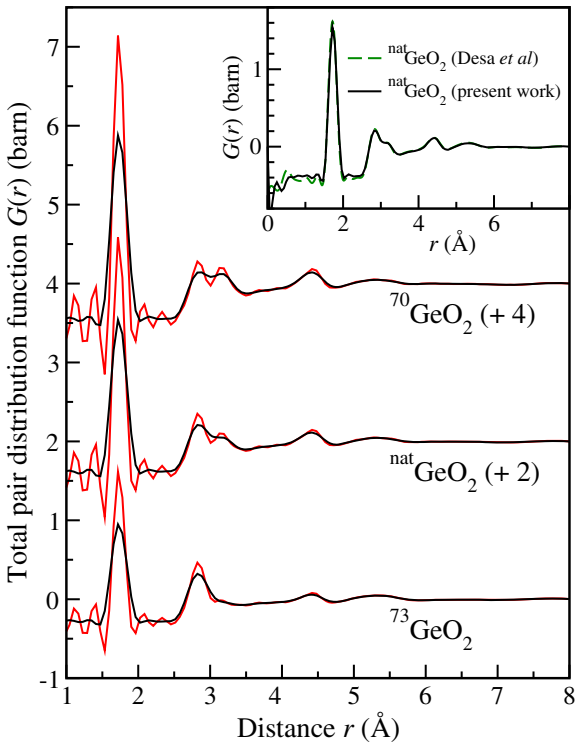

Figure 2. The measured total pair distribution functions $G(r)$ for glassy GeO_2. The functions were obtained by Fourier transforming the $F(k)$ shown in figure 1 after truncating either (i) abruptly by using a step function (solid light (red) curves) or (ii) smoothly by using a Lorch function (solid dark curves) with $k_{max} = 23.5$ Å^{-1} in both cases. The inset compares $^{nat}G(r)$ as measured in the present work (solid curve) with the results of Desa *et al* [52] (broken curve). Both data sets were obtained by Fourier transforming the measured $^{nat}F(k)$ after the application of a Lorch function with $k_{max} \approx 23.5$ Å^{-1}.

Table 1. Parameters obtained by fitting the Bhatia–Thornton pair correlation functions for glassy GeO_2. The $rh_{IJ}(r)$ functions were fitted by using equations (12)–(14) and the maxima in the $\ln|rh_{IJ}(r)|$ functions were fitted by using equation (15).

IJ	a_0 (Å^{-1})	a_0 [a] (Å^{-1})	a_1 (Å^{-1})	k_{PP} (Å^{-1})	A_{IJ} [b] (Å)	θ_{IJ} (rad)	R^2	Range (Å)
NN	0.33(3)	0.26(4)	2.78(3)	2.67(1)	2.1(8)	2.8(4)	0.86	12.3–19.9
CC	0.24(1)	0.25(2)	2.62(1)	2.65(1)	6.3(5)	−1.26(7)	0.94	4.7–15.4
NC	0.250(5)	0.26(1)	2.654(5)	2.66(1)	4.7(2)	1.66(5)	0.99	7.1–16.6

[a] From a straight line fit to the maxima in $\ln|rh_{IJ}(r)|$ versus r.
[b] $A_{NN} \equiv 2|\mathcal{A}_{NN}|$, $A_{CC} \equiv 2c_{Ge}c_O|\mathcal{A}_{CC}|$ and $A_{NC} \equiv 2|\mathcal{A}_{NC}|$.

account for the first order difference functions $\Delta F^{(i)}_{Ge}(k)$ and $\Delta G^{(i)}_{Ge}(r)$ (see figure 4) which is important because several types of systematic error are reduced or essentially eliminated when these difference functions are formed [54]. The results show that the FSDP in the measured $F(k)$, which is a ubiquitous feature of covalently bonded amorphous solids [55], appears at 1.53(2) Å^{-1} and has a notable contribution from all three $S_{\alpha\beta}(k)$. The principal peak in each function occurs at $k_{PP} \approx 2.66$ Å^{-1} (see table 1).

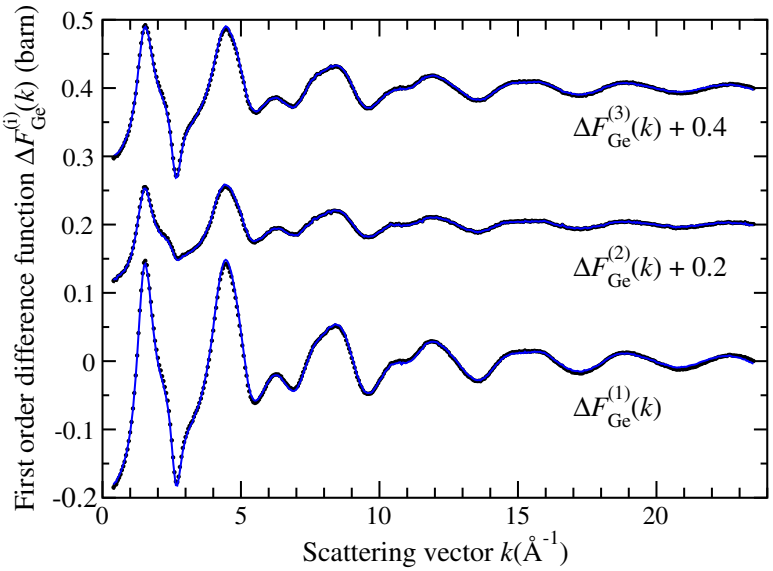

Figure 3. The measured first order difference functions $\Delta F_{\mathrm{Ge}}^{(i)}(k)$ ($i = 1, 2$ or 3) for glassy GeO_2. The solid circles give the data points and are larger than the statistical errors. The solid curves give the Fourier back-transforms of the corresponding $\Delta G_{\mathrm{Ge}}^{(i)}(r)$ functions after the small r oscillations are set equal to the limiting $\Delta G_{\mathrm{Ge}}^{(i)}(r = 0)$ value.

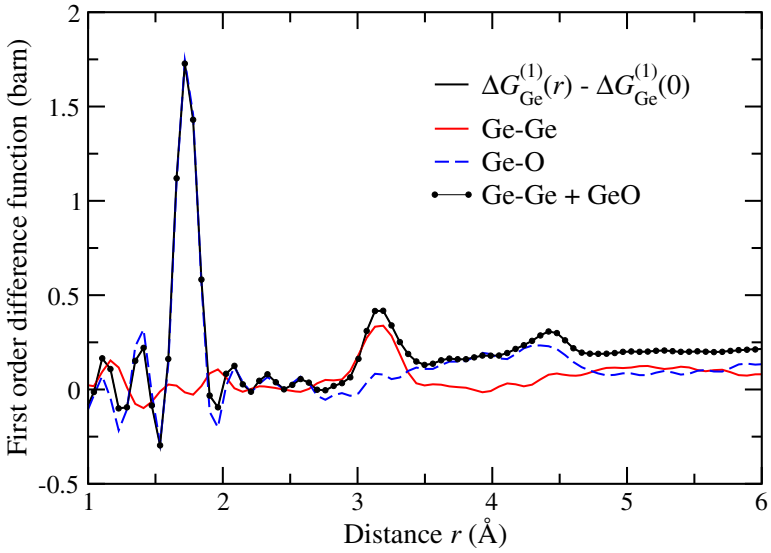

Figure 4. The measured first order difference function $\Delta G_{\mathrm{Ge}}^{(1)}(r)$ for glassy GeO_2 obtained by direct Fourier transformation of the $\Delta F_{\mathrm{Ge}}^{(1)}(k)$ function shown in figure 3 after the application of a step modification function with $k_{\max} = 23.5$ Å^{-1} (solid dark curve). The function is compared with the neutron weighted contributions from $g_{\mathrm{GeGe}}(r)$ (solid light (red) curve) and $g_{\mathrm{GeO}}(r)$ (broken (blue) curve) (see equation (7)). There is no significant discrepancy between $\Delta G_{\mathrm{Ge}}^{(1)}(r)$ and the weighted sum of the contributions from $g_{\mathrm{GeGe}}(r)$ and $g_{\mathrm{GeO}}(r)$ (solid circles).

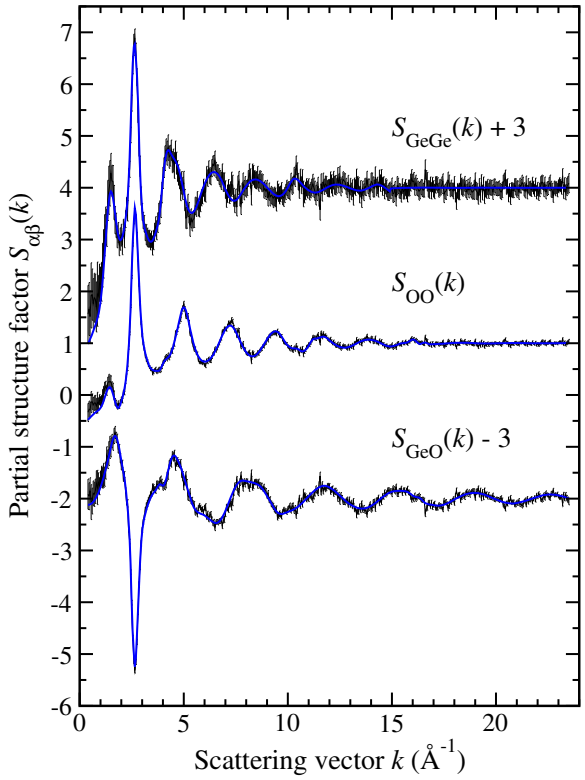

Figure 5. The measured Faber–Ziman partial structure factors $S_{\alpha\beta}(k)$ for glassy GeO_2 as represented by the points with error bars. The functions were obtained from the $F(k)$ shown in figure 1 by direct inversion of the scattering matrix (see equation (4)). The solid (blue) curves give the result of Fourier back-transforming the corresponding partial pair distribution functions, $g_{\alpha\beta}(r)$, which are shown in figure 6.

The $g_{\alpha\beta}(r)$ for glassy GeO_2 were obtained by Fourier transforming the measured $S_{\alpha\beta}(k)$ functions after they were spline fitted in order to reduce the effects of statistical noise. In the case of $g_{GeO}(r)$, a correction was also made for the effect of a step modification function $M(k)$ by assuming a Gaussian first peak in $d_{GeO}(r)$, convoluting this peak with the corresponding $M(r)$ function (see equation (9)), and fitting the result to the experimental data. The artifacts of $M(r)$ were thus identified and the fitted Gaussian was smoothly joined to the higher r features of the $d'_{GeO}(r)$ function obtained by direct Fourier transformation of the spline fitted $S_{\alpha\beta}(k)$. The $g_{\alpha\beta}(r)$ functions of figure 6 were thus obtained after setting the unphysical low r oscillations to zero. They were then Fourier transformed into k-space in order to confirm agreement with the measured $S_{\alpha\beta}(k)$ (see figure 5). Full details of the procedure used to extract $g_{GeO}(r)$ are described in [18].

5. Discussion

5.1. Structure of glassy GeO_2

The first peak in $g_{GeO}(r)$ at $r_{GeO} = 1.73(1)$ Å gives a coordination number $\bar{n}^{O}_{Ge} = 3.8(1)$. As in several other diffraction studies of GeO_2 [45, 52, 56], the measured Ge–O coordination number is systematically less than four owing to the finite k-space resolution function of the diffractometer for which a correction was not made [46, 57]. The first peak in $g_{OO}(r)$ at

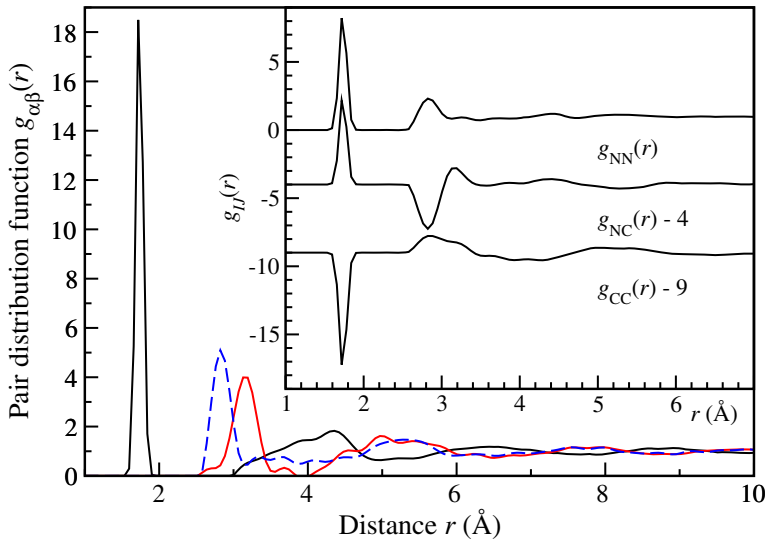

Figure 6. The measured partial pair distribution functions for glassy GeO_2. The main panel shows the functions $g_{GeO}(r)$ (solid black curve), $g_{GeGe}(r)$ (solid light (red) curve) and $g_{OO}(r)$ (broken (blue) curve). The inset shows the Bhatia–Thornton partial pair distribution functions which were obtained from the $g_{\alpha\beta}(r)$ functions of the main panel by using the relations $g_{NN}(r) = c_{Ge}^2 g_{GeGe}(r) + c_O^2 g_{OO}(r) + 2c_{Ge}c_O g_{GeO}(r)$, $g_{CC}(r) = c_{Ge}c_O[g_{GeGe}(r) + g_{OO}(r) - 2g_{GeO}(r)]$ and $g_{NC}(r) = c_{Ge}[g_{GeGe}(r) - g_{GeO}(r)] - c_O[g_{OO}(r) - g_{GeO}(r)]$ where $c_{Ge} = 1/3$ and $c_O = 2/3$.

$r_{OO}(r) = 2.83(1)$ Å gives a ratio $r_{OO}/r_{GeO} = 1.636(11)$ that is in agreement with the ideal tetrahedral ratio of $\sqrt{8/3} = 1.633$. The tetrahedra share corners to give 4.1(2) Ge–Ge nearest neighbours at $r_{GeGe} = 3.16(1)$ Å and there is an average of 6.7(1) O–O nearest neighbours for the range $2.58 \leqslant r$ (Å) $\leqslant 3.13$. In general, the packing fraction of X atoms of radius r_X in an AX_2 system is $\eta' = (8/9)n_0\pi r_X^3$ and for a perfect tetrahedron of four spherical touching X atoms, $r_{XX}/r_{AX} = \sqrt{8/3}$ where $r_{XX} = 2r_X$. Hence the packing fraction of X atoms in tetrahedral units, expressed as a function of r_{AX} and the atomic number density n_0, is $\eta' = 16\sqrt{2}\pi n_0 r_{AX}^3/27\sqrt{3} = 1.520 n_0 r_{AX}^3$ [58]. The packing fraction of oxygen atoms in tetrahedral units is thus found to be 0.495(9) in glassy GeO_2. A mean inter-tetrahedral Ge–Ô–Ge bond angle of 132(2)°, which is consistent with the literature [26, 38, 44, 59, 60], is obtained from the first Ge–O and Ge–Ge peak positions.

The measured Bhatia–Thornton partial structure factors $S_{IJ}(k)$ for glassy GeO_2 are shown in figure 7 and the corresponding partial pair distribution functions $g_{IJ}(r)$ are shown in the inset to figure 6. All of the $S_{IJ}(k)$ functions show a first sharp diffraction peak at $k_{FSDP} \approx 1.53$ Å^{-1} that is most prominent for $S_{NN}(k)$. The associated intermediate range order in real space [61] has a periodicity $2\pi/k_{FSDP}$ and coherence length $2\pi/\Delta k_{FSDP}$ where Δk_{FSDP} is the full width at half maximum of the FSDP. In the case of $S_{NN}(k)$, the periodicity and coherence length take values of 4.13(3) and 8.98(13) Å respectively. The $S_{CC}(k)$ and $S_{NC}(k)$ functions both show qualitative agreement with the corresponding functions for glassy $GeSe_2$ and $ZnCl_2$, which can be emphasized by plotting them against the reduced scattering vector kr_{AX} where r_{AX} is the separation of unlike nearest neighbours (see figure 2 in [19] and figure 1 in [33]). Intriguingly, $S_{CC}(k)$ shows a small but distinct FSDP which is indicative of concentration fluctuations on the scale of the intermediate range order [18, 47, 62]. This feature is not anticipated for strong glass forming systems such as GeO_2 and SiO_2 [63] and the origin of this feature for liquid and glassy $GeSe_2$ has proved difficult to trace [64–66]. It is now thought to result from coordination defects

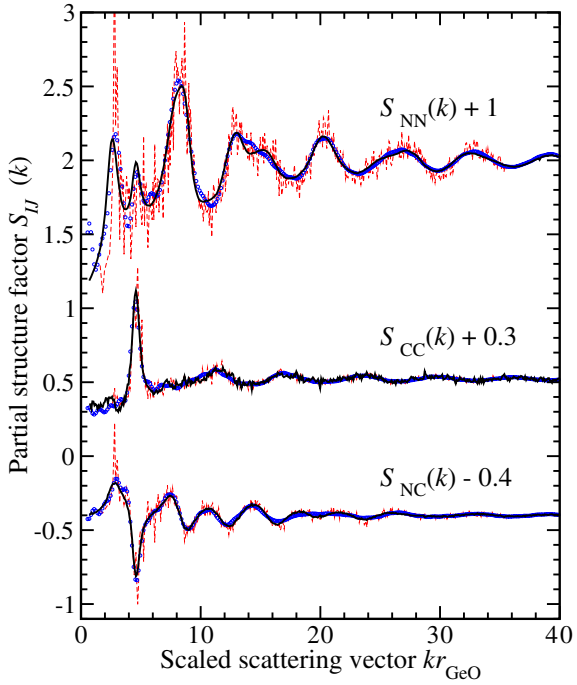

Figure 7. The measured Bhatia–Thornton partial structure factors, $S_{IJ}(k)$, for glassy GeO_2 (solid dark curves—the statistical uncertainties are represented by the scatter in the data points) compared with the first principles molecular dynamics results of Giacomazzi *et al* [38, 39] (broken (red) curves) and the molecular dynamics simulations of Micoulaut *et al* [35] (open (blue) circles). The partial structure factors are plotted as a function of the scaled scattering vector kr_{GeO} where r_{GeO} is the measured (1.73 Å) or calculated (1.78 Å for [38, 39] or 1.72 Å for [35]) nearest neighbour Ge–O distance. Each of the measured functions has an FSDP at $k \approx 1.53$ Å^{-1} or $kr_{GeO} \approx 2.65$.

and conformations of edge sharing tetrahedra [67, 68] that are not expected for GeO_2 [39]. The nature of the structural features in GeO_2 that are responsible for the FSDP in $S_{CC}(k)$ therefore requires further investigation. By contrast with the C–C and N–C partial structure factors, the partial structure factor describing the topological ordering, $S_{NN}(k)$, shows large differences between GeO_2 and both $GeSe_2$ and $ZnCl_2$ which are more intermediate in character on the fragility scale. In particular, the FSDP is stronger and the principal peak is weaker for GeO_2 compared with the other glasses [19, 33].

To examine further the differences between the topological and chemical ordering at distances greater than the nearest neighbour, it is useful to consider the theory for the asymptotic decay of the pair correlation functions developed by Evans and co-workers who made a pole analysis of the k-space solutions to the Ornstein–Zernike equations [69–72]. For a high density ionic AX_2 system described by pair potentials involving short ranged repulsive and long ranged Coulomb terms, the pair distribution functions at large distances are expected to decay as [46]

$$rh_{NN}(r) \rightarrow 2|\mathcal{A}_{NN}| \exp(-a_0 r) \cos(a_1 r - \theta_{NN}) \tag{12}$$

$$rh_{CC}(r) \rightarrow 2c_A c_X |\mathcal{A}_{CC}| \exp(-a_0 r) \cos(a_1 r - \theta_{CC}) \tag{13}$$

$$rh_{NC}(r) \rightarrow 2|\mathcal{A}_{NC}| \exp(-a_0 r) \cos(a_1 r - \theta_{NC}) \tag{14}$$

where $h_{NN}(r) = g_{NN}(r) - 1$, $h_{CC}(r) = g_{CC}(r)$ and $h_{NC}(r) = g_{NC}$. The amplitudes are related by $|\mathcal{A}_{NN}||\mathcal{A}_{CC}| = |\mathcal{A}_{NC}|^2$, the phases are related by $\theta_{NN} + \theta_{CC} = 2\theta_{NC}$, the common decay

length is given by a_0^{-1}, and the common wavelength of the oscillations is given by $2\pi/a_1$. Alternatively, if the pair potentials also include van der Waals (dispersion) terms with an r^{-6} dependence, a power law decay is ultimately expected where $rh_{\rm NN}(r) \to r^{-5}$, $rh_{\rm CC}(r) \to r^{-9}$ and $rh_{\rm NC}(r) \to r^{-7}$ [46, 73]. This power law decay might be difficult to observe owing to the relative weakness of the dispersion forces. However, the presence of these forces means that equations (12)–(14) will not necessarily hold since they were derived for the case when dispersion forces are absent. Furthermore, the presence of three or higher body interactions for glass forming AX_2 systems also provides complications but, provided the large r interactions can be described by effective pair potentials that lead to simple poles [46], it is feasible that the theory which leads to equations (12)–(14) will remain valid. Notwithstanding, these equations provide a benchmark for analysing the large r dependence of the Bhatia–Thornton pair distribution functions and for understanding the origin of extended range ordering in more complicated systems that involve three-body potentials.

The $h_{IJ}(r)$ functions for GeO_2 were obtained by spline fitting and Fourier transforming the $S_{IJ}(k)$ after (i) the low k data points ($k \leqslant 0.45$ Å^{-1}) were extrapolated to $k = 0$ by plotting either $[S_{\rm NN}(k) - 1]$, $[S_{\rm CC}(k)/c_{\rm Ge}c_{\rm O} - 1]$ or $S_{\rm NC}(k)/c_{\rm Ge}c_{\rm O}$ versus k^2 and fitting a straight line at small k [74] and (ii) a Lorch modification function was applied [45]. The resultant functions, plotted as $\ln|rh_{IJ}(r)|$ versus r in figure 8, show that the N–N correlations have a greater complexity than the N–C and C–C correlations over a wide range of distances and decay more rapidly at lower r values. All of the functions show extended range ordering at large r which persists to distances far exceeding the coherence length estimated from the width of an FSDP. The decay coefficients a_0 were estimated by fitting the repeated maxima at large r in figure 8, that are least sensitive to the details of any smoothing procedure, to the straight line

$$\ln|rh_{IJ}(r)| = -a_0 r + \text{constant}. \tag{15}$$

The $rh_{IJ}(r)$ functions were also fitted [46] by using equations (12)–(14) (see figure 8) and the fitted parameters, the range used for the fits, and the R^2 goodness-of-fit parameter are summarized in table 1. The a_0 values thus deduced represent upper limits owing to the k-space resolution function of the diffractometer [46]. The results show that the extended range oscillations for GeO_2 decay exponentially with a common decay coefficient a_0 and a periodicity that is determined not by the position of the FSDP but by the position of the principal peak i.e. the wavelength of the oscillations $2\pi/a_1 \approx 2\pi/k_{\rm PP}$. The relations between the amplitudes and phases predicted by the simple theory do not, however, appear to hold.

The values of the moments extracted from the small k fits to the $S_{IJ}(k)$ functions for glassy GeO_2 are not quoted since they are prone to systematic error [74]. For information, we note that the isothermal compressibility, $\kappa_{\rm T}$, of glassy GeO_2 at ambient pressure is 4.2×10^{-11} Pa^{-1} [75] and the measured refractive index for light of wavelength 0.589 29 μm is $n = 1.606\,86$ [76] which leads to a Debye screening length $\Lambda_{\rm D} = 0.027$ Å [74]. By assuming an ionic interaction model with Ge^{4+} ions of polarizability 0.60 Å^3 [77], use of this refractive index in the Clausius–Mossotti relation gives an O^{2-} ion polarizability of 1.67 Å^3.

5.2. Reconstruction of the x-ray and neutron total structure factors for glassy GeO_2 by using the measured $S_{\alpha\beta}(k)$

In order to interpret the x-ray diffraction data for glassy GeO_2 taken under ambient conditions and to aid in the interpretation of data taken under extreme conditions of temperature and pressure [13, 78, 79], it is instructive to investigate the contribution of the partial structure factors to the measured total x-ray structure factor where

$$S^{\rm X}(k) \equiv [F^{\rm X}(k) + \langle f(k)\rangle^2]/\langle f(k)\rangle^2. \tag{16}$$

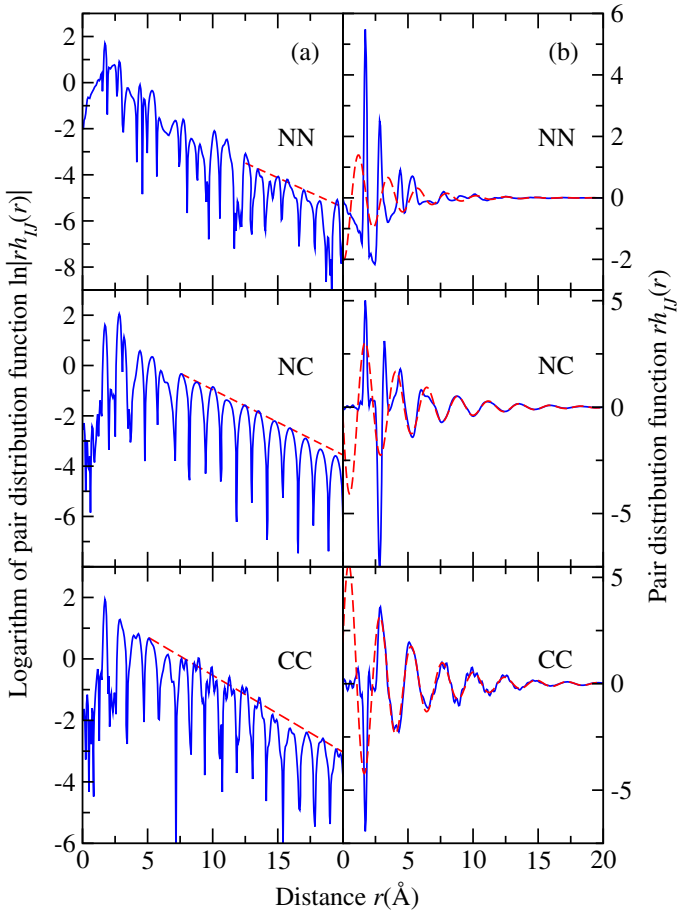

Figure 8. Decay of the Bhatia–Thornton partial pair distribution functions for glassy GeO_2 as shown by plotting $\ln|rh_{IJ}(r)|$ versus r (solid (blue) curves) in column (a) and $rh_{IJ}(r)$ versus r (solid (blue) curves) in column (b). For column (a), the coefficient a_0 was obtained from the fitted straight lines given by the broken (red) curves and for the N–N, N–C and C–C functions it takes values of 0.26(4) $Å^{-1}$ (fit range 12.5–19.6 Å, $R^2 = 0.87$), 0.26(1) $Å^{-1}$ (fit range 7.6–15.9 Å, $R^2 = 0.99$) and 0.25(2) $Å^{-1}$ (fit range 5.1–14.9 Å, $R^2 = 0.93$) respectively. For column (b), the broken (red) curves show the fits to the $rh_{IJ}(r)$ functions at large r values.

In this expression, $F^{X}(k)$ is given by equation (1) with b_{Ge} and b_O replaced by the x-ray form factors $f_{Ge}(k)$ and $f_O(k)$ for Ge and O respectively, and $\langle f(k)\rangle = c_{Ge} f_{Ge}(k) + c_O f_O(k)$. The $F^{X}(k)$ for glassy GeO_2 at ambient conditions, as measured by Sampath *et al* [78] using high energy x-ray diffraction, is illustrated in figure 9 together with its reconstruction from the x-ray weighted Faber–Ziman partial structure factors measured by neutron diffraction. Within the experimental error, agreement is found between the measured and reconstructed functions at all k values except the smallest where differences between the actual and tabulated [80] atomic form factors are expected to be greatest owing to the role of the outermost (valence) electrons in bonding. For comparison, the contribution of the $S_{\alpha\beta}(k)$ to the measured total neutron structure factor, $S^{N}(k)$, for $^{nat}GeO_2$ is shown in figure 10 where

$$^{nat}S^{N}(k) \equiv [^{nat}F(k) + \langle''b\rangle^2]/\langle''b\rangle^2, \tag{17}$$

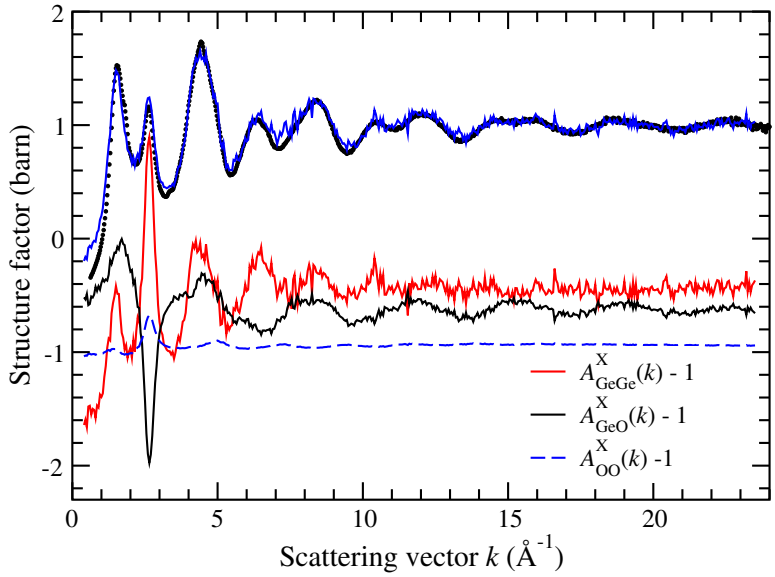

Figure 9. Reconstruction of the measured total x-ray structure factor $S^{X}(k) = A^{X}_{GeGe}(k) + A^{X}_{GeO}(k) + A^{X}_{OO}(k)$ for glassy GeO_2 [78] (solid circles) by using the x-ray weighted Faber–Ziman partial structure factors (solid (blue) curve). The contributions from the partial structure factors are given by $A^{X}_{GeGe}(k) = c^2_{Ge} f_{Ge}(k)^2 S_{GeGe}(k)/\langle f(k)\rangle^2$ (solid light (red) curve), $A^{X}_{GeO}(k) = 2c_{Ge}c_O f_{Ge}(k) f_O(k) S_{GeO}(k)/\langle f(k)\rangle^2$ (solid dark curve) and $A^{X}_{OO}(k) = c^2_O f_O(k)^2 S_{OO}(k)/\langle f(k)\rangle^2$ (broken (blue) curve) where the $S_{\alpha\beta}(k)$ are taken from figure 5, $\langle f(k)\rangle = c_{Ge} f_{Ge}(k) + c_O f_O(k)$, and the atomic form factors $f_{Ge}(k)$ and $f_O(k)$ are taken from [80]. The statistical uncertainties are represented by the scatter in the data points.

$\langle''b\rangle = c_{Ge}\,''b_{Ge} + c_O b_O$ and $''b_{Ge} = b(^{nat}Ge)$. In this expression, the weighting coefficients for the Ge–Ge, Ge–O and O–O partial structure factors are independent of k and take values of 0.1710, 0.4851 and 0.3439 respectively.

A comparison of the results given in figures 9 and 10 show that, although the O–O correlations have a larger weighting in $^{nat}S^{N}(k)$ compared with $S^{X}(k)$, the Ge–Ge and Ge–O correlations still give the largest contribution to $^{nat}S^{N}(k)$ in the region of the FSDP. It is therefore unsafe to attribute the changes observed with increasing pressure in the FSDP region for $S^{X}(k)$ and $^{nat}S^{N}(k)$ to changes that are mostly associated with the oxygen atom correlations [13]. The small principal peak observed in $^{nat}S^{N}(k)$ (figure 10) arises from an almost complete cancellation of the large principal peaks in the neutron weighted $S_{\alpha\beta}(k)$.

5.3. Comparison between the measured and simulated structure of glassy GeO_2

The measured partial structure factors and pair distribution functions are compared with the results from two recent molecular dynamics simulations in figures 7, 11 and 12. The first set of simulations were made by Micoulaut *et al* [34, 35, 37] using the two body potential developed by Oeffner and Elliott for GeO_2 [81] and classical molecular dynamics (a similar approach was adopted by Gutiérrez and Rogan [82] to study the density dependent structure of the liquid phase of GeO_2). The second set of simulations were made by Giacomazzi *et al* using first principles molecular dynamics [38, 39]. Compared to experiment, both sets of simulations give a higher first peak in $g_{GeO}(r)$ (24.4 [35] and 20.3 [38, 39] cf. 18.5) which yields a larger Ge–O coordination number of four, features that can be attributed to the k-space resolution

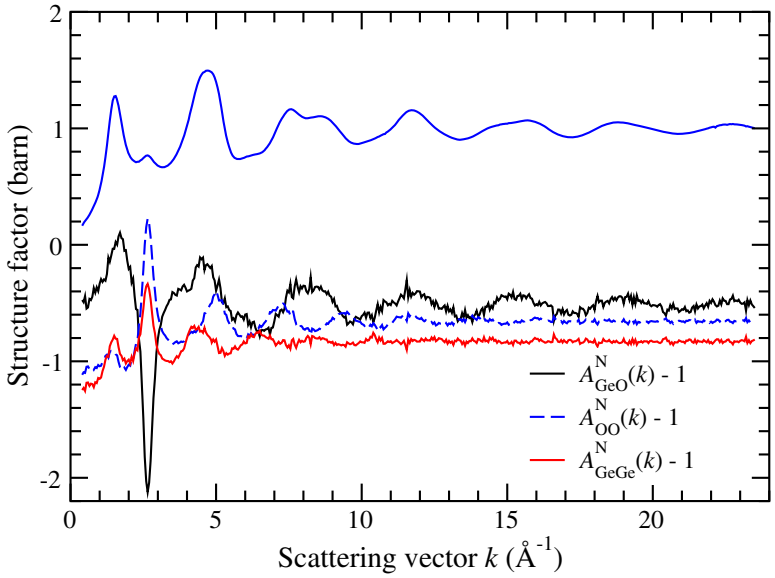

Figure 10. The contribution to the measured total neutron structure factor $^{nat}S^{N}(k) = A^{N}_{GeGe}(k) + A^{N}_{GeO}(k) + A^{N}_{OO}(k)$ for glassy $^{nat}GeO_2$ (solid (blue) curve) from the neutron weighted Faber–Ziman partial structure factors where $A^{N}_{GeGe}(k) = c^2_{Ge}{''b}^2_{Ge}S_{GeGe}(k)/\langle{''b}\rangle^2$ (solid light (red) curve), $A^{N}_{GeO}(k) = 2c_{Ge}c_O{''b}_{Ge}b_O S_{GeO}(k)/\langle{''b}\rangle^2$ (solid dark curve) and $A^{N}_{OO}(k) = c^2_O b^2_O S_{OO}(k)/\langle{''b}\rangle^2$ (broken (blue) curve). The $S_{\alpha\beta}(k)$ are taken from figure 5, $\langle{''b}\rangle = c_{Ge}{''b}_{Ge} + c_O b_O$, ${''b}_{Ge}$ is the bound coherent scattering length of ^{nat}Ge, and the measured $^{nat}S^{N}(k)$ function is reproduced by the sum of the $A^{N}_{\alpha\beta}(k)$. The statistical uncertainties are represented by the scatter in the data points.

function of the diffractometer used in the experiments [46, 57]. Although a correction for the resolution function was not made, one approach to this problem lies in the 'moments method' of Howells [83] which has been successfully applied to the case of liquid lithium [84]. The first peak positions and coordination numbers obtained from the $g_{\alpha\beta}(r)$ functions are compared with experiment in table 2. The experimental values obtained from the present work are in excellent accord with the results obtained from previous diffraction experiments (see table 1 in [31]), with the exception of $\bar{n}^{O}_{O}$ for which a value greater than six was obtained directly from the measured $g_{OO}(r)$ function and not from a peak fitting procedure as used in previous work. The first principles results give an elongated peak position of $r_{GeO} = 1.78$ Å attributed to the use of a generalized gradient approximation in the electronic structure calculations, which has prompted the use of a scaled abscissa in figures 7, 11 and 12. The mean inter-tetrahedral Ge–Ô–Ge bond angle of 132(2)° obtained from experiment compares with 159° [35] and 135° [38, 39]. Overall, there is good agreement between the measured and simulated pair correlation functions although some important discrepancies occur.

For the classical molecular dynamics results, the most notable disagreement with experiment manifests itself in a shift to high k of the FSDP position and reduction of the principal peak height in the simulated $S_{GeGe}(k)$, a phase shift of the higher k oscillations in this function (figure 11), a reduction in height and shift to high r of the first peak in the simulated $g_{GeGe}(r)$, and a much broader distribution of the other features in this function (figure 12). In consequence, the Ge–Ô–Ge bond angle is too large and the relative distribution of the centres of the $Ge(O_{1/2})_4$ tetrahedra on an intermediate length scale is not correctly described, thus leading to systematic errors in a description of the topological ordering [37]. The failure to

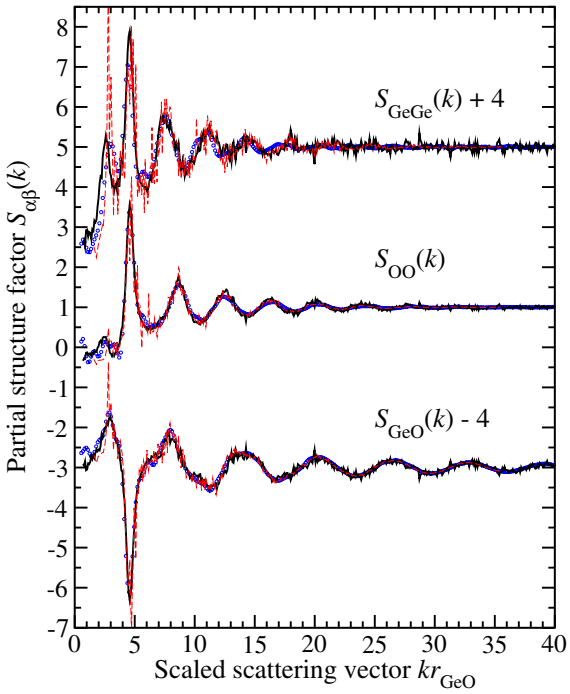

Figure 11. Comparison of the measured Faber–Ziman partial structure factors, $S_{\alpha\beta}(k)$, for glassy GeO_2 (solid dark curves) with the first principles molecular dynamics results of Giacomazzi *et al* [38, 39] (broken (red) curves) and the molecular dynamics simulations of Micoulaut *et al* [35] (open (blue) circles). The data sets are plotted as a function of the scaled scattering vector kr_{GeO} where r_{GeO} is the measured (1.73 Å) or calculated (1.78 Å for [38, 39] or 1.72 Å for [35]) nearest neighbour Ge–O distance.

Table 2. Parameters obtained from the first peak in the measured and simulated $g_{\alpha\beta}(r)$ for glassy GeO_2. The coordination numbers were calculated using a cut-off value equal to the minimum after the first main peak in $g_{\alpha\beta}(r)$.

Correlation α–β	$r_{\alpha\beta}$ (Å)	$\bar{n}_\alpha^\beta$	Range (Å)	Reference
GeO	1.73(1)	3.8(1)	1.53–1.96	Present work
	1.72	4.1	1.60–2.30	[35]
	1.69	4.00	1.5–2.2	[36]
	1.78	4.01	1.53–2.25	[39]
GeGe	3.16(1)	4.1(2)	2.58–3.56	Present work
	3.32	4.4	2.20–3.60	[35]
	3.21	4.06	2.7–3.6	[36]
	3.25	4.1	2.70–3.73	[39]
OO	2.83(1)	6.7(1)	2.58–3.13	Present work
	2.81	8.2	2.25–3.30	[35]
	2.78	6.44	2.5–3.2	[36]
	2.88	7.8	2.11–3.40	[39]

reproduce these experimental features may help to account for the severe over estimation of the self-diffusion coefficients obtained from simulations of the molten phase [35]. Classical molecular dynamics simulations of glassy GeO_2 have also been made using a pair potential with

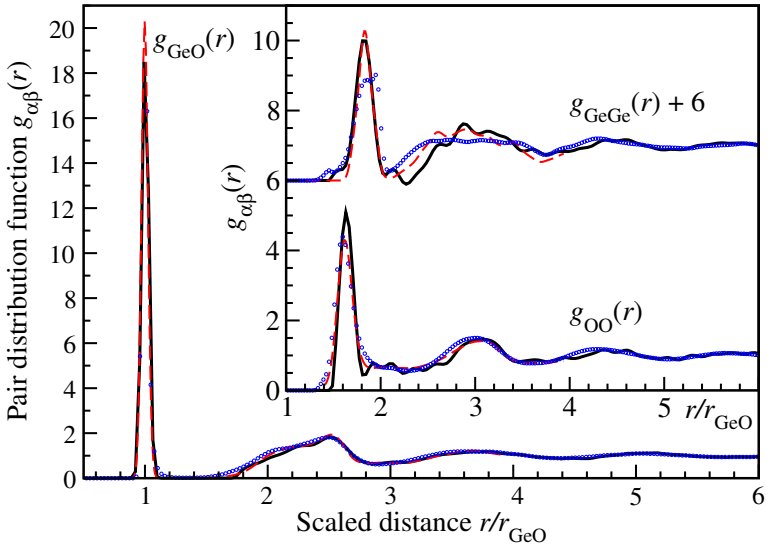

Figure 12. Comparison of the measured partial pair distribution functions, $g_{\alpha\beta}(r)$, for glassy GeO_2 (solid dark curves) with the first principles molecular dynamics results of Giacomazzi *et al* [38, 39] (broken (red) curves) and the molecular dynamics simulations of Micoulaut *et al* [35] (open (blue) circles). The data sets are plotted as a function of the scaled distance r/r_{GeO} where r_{GeO} is the measured (1.73 Å) or calculated (1.78 Å for [38, 39] or 1.72 Å for [35]) nearest neighbour Ge–O distance.

a Morse-type short ranged term [36] and give an improved Ge–Ge nearest neighbour distance and Ge–Ô–Ge bond angle of 133° although the Ge–O and O–O distances are too small (see table 2). The diffusion coefficients calculated for the liquid phase are significantly smaller than those obtained in [35], in better agreement with experiment.

For the first principles molecular dynamics results, the agreement with experiment is improved although the small number of atoms used in the simulation (168) leads to large statistical uncertainties in the region of the FSDP [38, 39]. A small FSDP in $S_{CC}(k)$ is nevertheless found, in agreement with experiment (figure 7). In real space, the most notable discrepancies between the first principles and experimental results (figure 12) occur with respect to the relative sharpness of the measured first peak in $g_{OO}(r)$ and the small mismatch between the measured and simulated $g_{GeGe}(r)$ in the second peak region. The vibrational properties of the simulated network give spectra that are in good overall agreement with those measured by using inelastic neutron scattering, infrared spectroscopy and Raman scattering. The theoretical spectra do, however, show an overall shift to lower frequencies which is attributed to the use of a generalized gradient approximation in the set-up of the density functional theory [38].

5.4. Relation between the structure and fragility of AX_2 glass forming systems

To investigate the relation between the structure of GeO_2 and other *strong* network forming AX_2 glasses based on tetrahedral $A(X_{1/2})_4$ units, the total structure factor for SiO_2, $F_{Si}(k)$, was measured in the *same* neutron diffraction experiment used to obtain the partial structure factors for GeO_2. Silica is often regarded as the canonical network forming glass and is of wide scientific and technological significance [1, 14]. The total structure factor for silica was then reconstructed by using the measured $S_{\alpha\beta}(k)$ for germania where $F_{Si}^{rec}(k) = c_{Si}^2 b_{Si}^2 [S_{GeGe}(k) -$

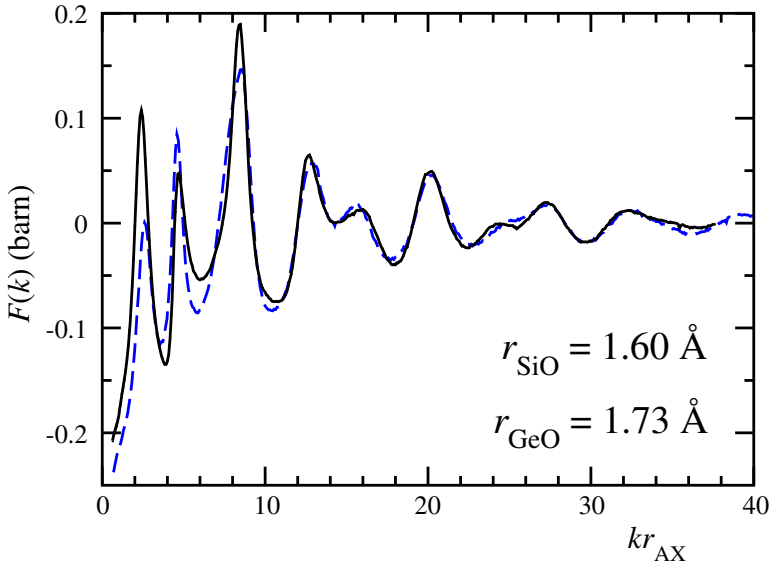

Figure 13. The measured total structure factor for glassy SiO_2, $F_{Si}(k)$, (solid curve with vertical error bars—the latter are smaller than the curve thickness at all k values) compared with its reconstruction, $F_{Si}^{rec}(k)$, (broken curve) from the measured partial structure factors for glassy GeO_2 given in figure 5 (see text). Both data sets are plotted as a function of the scaled scattering vector kr_{AX} where r_{AX} is the separation of unlike nearest neighbours.

$1]+2c_{Si}c_O b_{Si}b_O[S_{GeO}(k)-1]+c_O^2 b_O^2[S_{OO}(k)-1]$ and $b_{Si} = 4.1491(10)$ fm [42]. The measured $F_{Si}(k)$ and its reconstruction $F_{Si}^{rec}(k)$ are shown in figure 13 and the corresponding Fourier transforms, the total pair distribution functions $G_{Si}(r)$ and $G_{Si}^{rec}(r)$, are shown in figure 14. In these figures, scaled abscissae of kr_{AX} and r/r_{AX} are used, where r_{AX} is the nearest neighbour bond length, to provide the best match between the data sets.

The structure of silica is also based on an open network of corner sharing $A(X_{1/2})_4$ tetrahedra, where the nearest neighbour Si–O and O–O distances are 1.60(1) and 2.62(1) Å respectively (see figure 14). The mean inter-tetrahedral bond angle Si–Ô–Si is, however, larger at 148° [60] and the packing fraction of the oxygen atoms is smaller at $\eta' = 0.414(8)$. The relative arrangement of the $A(X_{1/2})_4$ tetrahedra is therefore different and manifests itself on both the intermediate and extended range as shown by a higher and sharper FSDP in $F_{Si}(k)$ compared with $F_{Si}^{rec}(k)$ together with a lower and broader principal peak. Neutron scattering studies hint at concomitant differences between the microscopic dynamics of GeO_2 and SiO_2 in the liquid phase [85]. The same general features nevertheless occur in the total structure factors and pair distribution functions for both strong glasses.

Polyamorphic phase transitions are often associated with a distinct change in the structure of a liquid or glass from strong to fragile with increase of density [4, 14, 15] and tetrahedrally bonded systems remain the most promising candidates for studying this phenomenon experimentally [86, 87]. Furthermore, two or more competing length scales are built into simple model pair potentials that are used in calculations to examine the feasibility of liquid–liquid phase transitions [88–90].

A comparison of the present results with those for glassy $ZnCl_2$ [19] show that it is the relative importance of the FSDP and principal peak that most readily enables a distinction to be made between the diffraction patterns measured for the strong glass GeO_2 and the intermediate glass $ZnCl_2$—the FSDP in $S_{NN}(k)$ for $ZnCl_2$ is much smaller and the principal peak is much

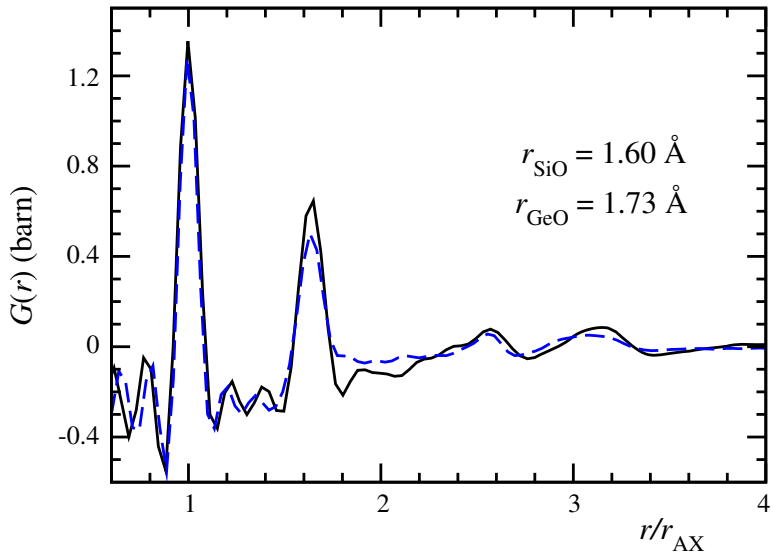

Figure 14. The measured total pair distribution function, $G_{\rm Si}(r)$, for glassy SiO_2 (solid curve) compared with its reconstruction, $G^{\rm rec}_{\rm Si}(r)$, from the data for glassy GeO_2 (broken curve). Both functions were obtained by Fourier transforming the total structure factors shown in figure 13 by using a step function with $k_{\rm max} = 23.5$ Å^{-1} and are plotted as a function of the scaled distance $r/r_{\rm AX}$.

larger than for GeO_2 (see figure 1 of [33]). Like GeO_2, the network of glassy $ZnCl_2$ is also made from corner sharing $A(X_{1/2})_4$ tetrahedra but the mean inter-tetrahedral bond angle Zn–$\hat{\rm Cl}$–Zn is smaller at 111(1)° and the anion packing fraction is much higher at $\eta' = 0.647(9)$. Although homopolar bonds and edge sharing $A(X_{1/2})_4$ tetrahedra are a feature of glassy $GeSe_2$ [17, 18], the measured $S_{IJ}(k)$ are comparable to those for glassy $ZnCl_2$ (see figure 2 of [19]) with an FSDP and principal peak that are a little sharper and a little weaker, respectively. On the fragility scale, $GeSe_2$ is also more intermediate in character than GeO_2 [91] and, if the influence of homopolar bonds is ignored, an anion packing fraction $\eta' = 0.667(17)$ is found using $r_{\rm GeSe} = 2.36(2)$ Å with a mean inter-tetrahedral bond angle Ge–$\hat{\rm Se}$–Ge of 98(1)°. When glassy $GeSe_2$ is subjected to a pressure increasing from ambient to 9.3 GPa, the FSDP in $S_{\rm NN}(k)$ vanishes and the principal peak gains in intensity [92]. Similar behaviour for $S_{\rm NN}(k)$ is observed for the liquid phase of $GeSe_2$ as the density is increased at constant temperature by applying a pressure between 0.5 and 4.1 GPa at 1120 K [93]. When the temperature of liquid $GeSe_2$ is increased at much lower pressures, the density also *increases* as the network collapses [94]. The FSDP in $S_{\rm NN}(k)$ diminishes in intensity relative to the principal peak and shifts to higher k values as the temperature is raised to 1100 °C and the observed trend in the overall shape of $S_{\rm NN}(k)$ [95] mimics that found in the liquid phase as Ge is added to $GeSe_2$ to form GeSe [96]. In both situations, the $Ge(Se_{1/2})_4$ tetrahedra are broken down [97, 98].

When pressures up to 15 GPa are applied to GeO_2, x-ray and neutron diffraction experiments show that the FSDP moves to higher k and merges with the principal peak as the network first collapses and the germanium coordination number eventually increases [13], thus enhancing the relative importance of the principal peak. For silica, the measured diffraction pattern features a more prominent FSDP and weaker principal peak (see figure 13) and much higher pressures are required to induce a network collapse compared to germania [11, 13]. Hence there is a competition between the intermediate and extended range ordering in

tetrahedral network forming AX_2 glasses, the former being favoured for open network structures with large A–$\hat{X}$–A inter-tetrahedral bond angles and the latter being favoured for close packed structures when A–$\hat{X}$–A is correspondingly small. This competition is won by the extended range ordering when the density is increased and the system becomes more fragile.

6. Conclusions

The full set of partial structure factors has been accurately measured for glassy GeO_2 by using the method of isotopic substitution in neutron diffraction. The results show that the network structure is based on corner sharing $Ge(O_{1/2})_4$ tetrahedra with a mean inter-tetrahedral Ge–$\hat{O}$–Ge bond angle of 132(2)°. The measured $S_{\alpha\beta}(k)$ can be used to reproduce the structure factor measured by using high energy x-ray diffraction and a comparison with molecular dynamics simulations shows that improved models for the network structure can be developed. The results suggest that there is a competition between the intermediate and extended range ordering in network AX_2 glasses that is won by the latter with increasing glass fragility.

Acknowledgments

It is a pleasure to thank Pierre Palleau for help with the diffraction experiment, Adrian Wright and Chris Benmore for providing their diffraction data for GeO_2, Luigi Giacomazzi and Matthieu Micoulaut for providing their molecular dynamics results for GeO_2, and the EPSRC for financial support. It is also a pleasure for Phil Salmon and Adrian Barnes to express their sincere gratitude to Spencer Howells for all his invaluable help, advice and friendship over many years.

References

[1] Angell C A 1995 *Science* **267** 1924
[2] Debenedetti P G 1996 *Metastable Liquids* (Princeton, NJ: Princeton University Press) p 301
[3] Sciortino F, Kob W and Tartaglia P 1999 *Phys. Rev. Lett.* **83** 3214
[4] Sastry S 2001 *Nature* **409** 164
[5] Saksaengwijit A, Reinisch J and Heuer A 2004 *Phys. Rev. Lett.* **93** 235701
[6] Moreno A J, Buldyrev S V, La Nave E, Saika-Voivod I, Sciortino F, Tartaglia P and Zaccarelli E 2005 *Phys. Rev. Lett.* **95** 157802
[7] Scopigno T, Ruocco G, Sette F and Monaco G 2003 *Science* **302** 849
[8] Novikov V N and Sokolov A P 2004 *Nature* **431** 961
[9] Yannopoulos S N and Johari G P 2006 *Nature* **442** E7
[10] Itie J P, Polian A, Calas G, Petiau J, Fontaine A and Tolentino H 1989 *Phys. Rev. Lett.* **63** 398
[11] Durben D J and Wolf G H 1991 *Phys. Rev.* B **43** 2355
[12] Polsky C H, Smith K H and Wolf G H 1999 *J. Non-Cryst. Solids* **248** 159
[13] Guthrie M, Tulk C A, Benmore C J, Xu J, Yarger J L, Klug D D, Tse J S, Mao H-k and Hemley R J 2004 *Phys. Rev. Lett.* **93** 115502
[14] Saika-Voivod I, Poole P H and Sciortino F 2001 *Nature* **412** 514
[15] Saika-Voivod I, Sciortino F and Poole P H 2004 *Phys. Rev.* E **69** 041503
[16] Angell C A 1985 *J. Non-Cryst. Solids* **73** 1
[17] Petri I, Salmon P S and Fischer H E 2000 *Phys. Rev. Lett.* **84** 2413
[18] Salmon P S and Petri I 2003 *J. Phys.: Condens. Matter* **15** S1509
[19] Salmon P S, Martin R A, Mason P E and Cuello G J 2005 *Nature* **435** 75
[20] Bhatia A B and Thornton D E 1970 *Phys. Rev.* B **2** 3004
[21] Foley M, Wilson M and Madden P A 1995 *Phil. Mag.* B **71** 557
[22] Fischer H E, Cuello G J, Palleau P, Feltin D, Barnes A C, Badyal Y S and Simonson J M 2002 *Appl. Phys.* A **74** S160
[23] Enderby J E, North D M and Egelstaff P A 1966 *Phil. Mag.* **14** 961
[24] Bondot P 1974 *Acta Crystallogr.* A **30** 470

[25] Waseda Y, Sugiyama K, Matsubara E and Harada K 1990 *Mater. Trans. JIM* **31** 421
[26] Price D L, Saboungi M-L and Barnes A C 1998 *Phys. Rev. Lett.* **81** 3207
[27] Kang S, Park C, Saito M and Waseda Y 1999 *Mater. Trans. JIM* **40** 552
[28] Kohara S and Suzuya K 2003 *Nucl. Instrum. Methods Phys. Res.* B **199** 23
[29] Kohara S and Suzuya K 2005 *J. Phys.: Condens. Matter* **17** S77
[30] McGreevy R L 2001 *J. Phys.: Condens. Matter* **13** R877
[31] Micoulaut M, Cormier L and Henderson G S 2006 *J. Phys.: Condens. Matter* **18** R753
[32] Dianov E M and Mashinsky V M 2005 *J. Lightwave Technol.* **23** 3500
[33] Salmon P S, Barnes A C, Martin R A and Cuello G J 2006 *Phys. Rev. Lett.* **96** 235502
[34] Micoulaut M 2004 *J. Phys.: Condens. Matter* **16** L131
[35] Micoulaut M, Guissani Y and Guillot B 2006 *Phys. Rev.* E **73** 031504
[36] Van Hoang V 2006 *J. Phys.: Condens. Matter* **18** 777
[37] Micoulaut M, Yuan X and Hobbs L W 2007 *J. Non-Cryst. Solids* **353** 1961
[38] Giacomazzi L, Umari P and Pasquarello A 2005 *Phys. Rev. Lett.* **95** 075505
[39] Giacomazzi L, Umari P and Pasquarello A 2006 *Phys. Rev.* B **74** 155208
[40] Fischer H E, Barnes A C and Salmon P S 2006 *Rep. Prog. Phys.* **69** 233
[41] Faber T E and Ziman J M 1965 *Phil. Mag.* **11** 153
[42] Sears V F 1992 *Neutron News* **3** 26
[43] Edwards F G, Enderby J E, Howe R A and Page D I 1975 *J. Phys. C: Solid State Phys.* **8** 3483
[44] Leadbetter A J and Wright A C 1972 *J. Non-Cryst. Solids* **7** 37
[45] Lorch E 1969 *J. Phys. C: Solid State Phys.* **2** 229
[46] Salmon P S 2006 *J. Phys.: Condens. Matter* **18** 11443
[47] Salmon P S 1992 *Proc. R. Soc.* A **437** 591
[48] Vergano P J and Uhlmann D R 1970 *Phys. Chem. Glasses* **11** 30
[49] Jal J F, Mathieu C, Chieux P and Dupuy J 1990 *Phil. Mag.* B **62** 351
[50] Bertagnolli H, Chieux P and Zeidler M D 1976 *Mol. Phys.* **32** 759
[51] Salmon P S 1988 *J. Phys. F: Met. Phys.* **18** 2345
[52] Desa J A E, Wright A C and Sinclair R N 1988 *J. Non-Cryst. Solids* **99** 276
[53] Salmon P S and Benmore C J 1992 *Recent Developments in the Physics of Fluids* ed W S Howells and A K Soper (Bristol: Hilger) p F225
[54] Salmon P S, Xin S and Fischer H E 1998 *Phys. Rev.* B **58** 6115
[55] Elliott S R 1991 *Nature* **354** 445
[56] Price D L, Ellison A J G, Saboungi M-L, Hu R-Z, Egami T and Howells W S 1997 *Phys. Rev.* B **55** 11249
[57] Grimley D I, Wright A C and Sinclair R N 1990 *J. Non-Cryst. Solids* **119** 49
[58] Wright A C, Etherington G, Desa J A E, Sinclair R N, Connell G A N and Mikkelsen J C Jr 1982 *J. Non-Cryst. Solids* **49** 63
[59] Hussin R, Dupree R and Holland D 1999 *J. Non-Cryst. Solids* **246** 159
[60] Neuefeind J and Liss K-D 1996 *Ber. Bunsenges. Phys. Chem.* **100** 1341
[61] Salmon P S 1994 *Proc. R. Soc.* A **445** 351
[62] Penfold I T and Salmon P S 1991 *Phys. Rev. Lett.* **67** 97
[63] Massobrio C, Celino M and Pasquarello A 2004 *Phys. Rev.* B **70** 174202
[64] Massobrio C, Pasquarello A and Car R 1998 *Phys. Rev. Lett.* **80** 2342
[65] Massobrio C, Pasquarello A and Car R 2001 *Phys. Rev.* B **64** 144205
[66] Massobrio C and Pasquarello A 2003 *Phys. Rev.* B **68** 020201
[67] Sharma B K and Wilson M 2006 *Phys. Rev.* B **73** 060201
[68] Massobrio C and Pasquarello A 2007 *Phys. Rev.* B **75** 014206
[69] Evans R, Leote de Carvalho R J F, Henderson J R and Hoyle D C 1994 *J. Chem. Phys.* **100** 591
[70] Leote de Carvalho R J F and Evans R 1994 *Mol. Phys.* **83** 619
[71] Leote de Carvalho R J F, Evans R, Hoyle D C and Henderson J R 1994 *J. Phys.: Condens. Matter* **6** 9275
[72] Grodon C, Dijkstra M, Evans R and Roth R 2004 *J. Chem. Phys.* **121** 7869
[73] Kjellander R and Forsberg B 2005 *J. Phys. A: Math. Gen.* **38** 5405
[74] Salmon P S 2005 *J. Phys.: Condens. Matter* **17** S3537
[75] Smith K H, Shero E, Chizmeshya A and Wolf G H 1995 *J. Chem. Phys.* **102** 6851
[76] Polukhin V N 1982 *Fiz. Khim. Stekla* **8** 338
[77] Duffy J A 2005 *Phys. Chem. Glasses* **46** 1
[78] Sampath S, Benmore C J, Lantzky K M, Neuefeind J, Leinenweber K, Price D L and Yarger J L 2003 *Phys. Rev. Lett.* **90** 115502
[79] Hong X, Shen G, Prakapenka V B, Newville M, Rivers M L and Sutton S R 2007 *Phys. Rev.* B **75** 104201

[80] Maslen E N, Fox A G and O'Keefe M A 1995 *International Tables for Crystallography* vol C ed A J C Wilson (Dordrecht: Kluwer) p 476 (section 6.1.1)
[81] Oeffner R D and Elliott S R 1998 *Phys. Rev.* B **58** 14791
[82] Gutiérrez G and Rogan J 2004 *Phys. Rev.* E **69** 031201
[83] Howells W S 1984 *Nucl. Instrum. Methods Phys. Res.* **219** 543
[84] Salmon P S, Petri I, de Jong P H K, Verkerk P, Fischer H E and Howells W S 2004 *J. Phys.: Condens. Matter* **16** 195
[85] Meyer A, Schober H and Neuhaus J 2001 *Phys. Rev.* B **63** 212202
[86] Poole P H, Grande T, Angell C A and McMillan P F 1997 *Science* **275** 322
[87] Wilding M C, Wilson M and McMillan P F 2006 *Chem. Soc. Rev.* **35** 964
[88] Franzese G, Malescio G, Skibinsky A, Buldyrev S V and Stanley H E 2001 *Nature* **409** 692
[89] Jagla E A 2001 *Phys. Rev.* E **63** 061501
[90] Gibson H M and Wilding N B 2006 *Phys. Rev.* E **73** 061507
Gibson H M and Wilding N B 2006 *Phys. Rev.* E **74** 019903
[91] Stølen S, Grande T and Johnsen H-B 2002 *Phys. Chem. Chem. Phys.* **4** 3396
[92] Mei Q, Benmore C J, Hart R T, Bychkov E, Salmon P S, Martin C D, Michel F M, Antao S M, Chupas P J, Lee P L, Shastri S D, Parise J B, Leinenweber K, Amin S and Yarger J L 2006 *Phys. Rev.* B **74** 014203
[93] Crichton W A, Mezouar M, Grande T, Stølen S and Grzechnik A 2001 *Nature* **414** 622
[94] Ruska J and Thurn H 1976 *J. Non-Cryst. Solids* **22** 277
[95] Petri I, Salmon P S and Howells W S 1999 *J. Phys.: Condens. Matter* **11** 10219
[96] Salmon P S and Liu J 1994 *J. Phys.: Condens. Matter* **6** 1449
[97] Petri I, Salmon P S and Fischer H E 1999 *J. Phys.: Condens. Matter* **11** 7051
[98] Massobrio C, van Roon F H M, Pasquarello A and De Leeuw S W 2000 *J. Phys.: Condens. Matter* **12** L697